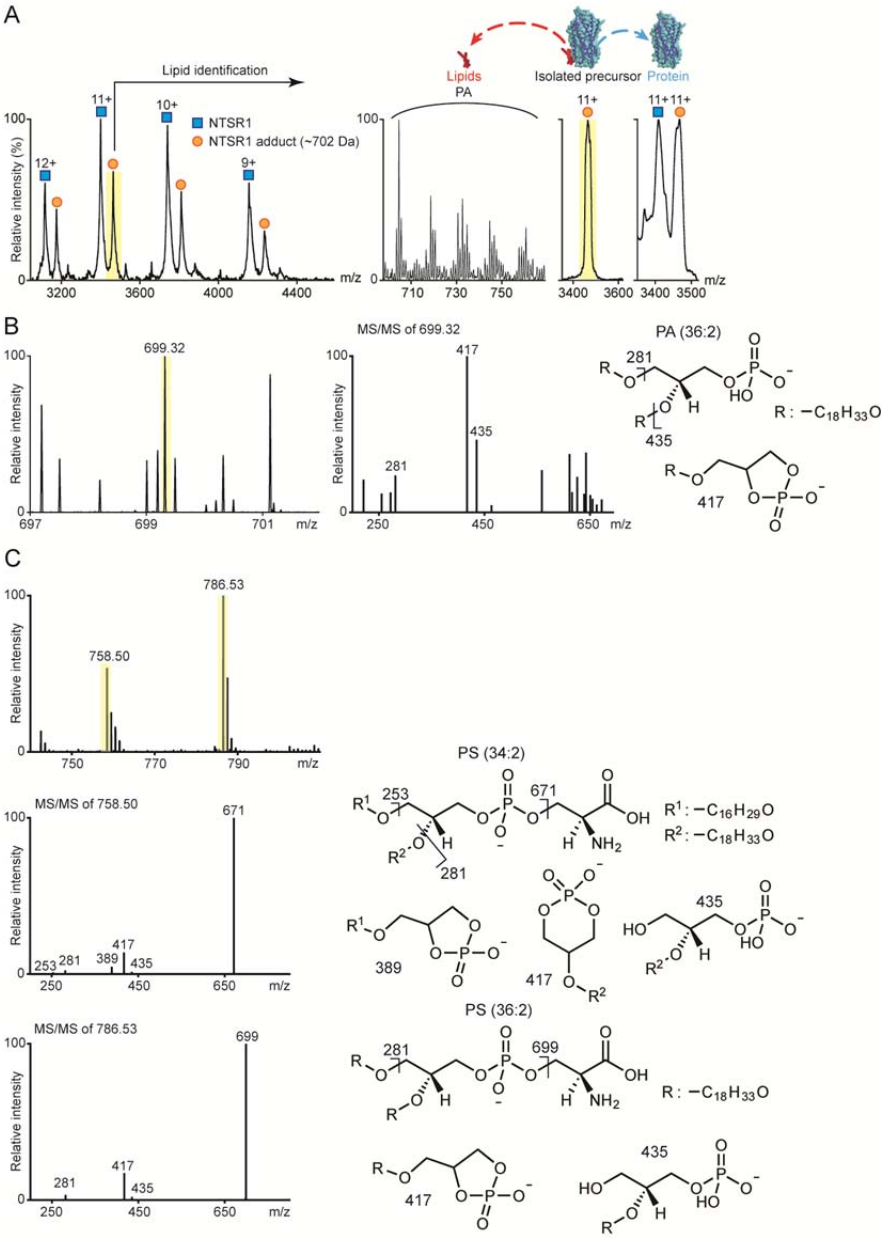

Extended Data Figure 1. Identification of lipids bound to NTSR1 HTGH4-ΔIC3B. a, Endogenous lipid bounds to NTSR1 HTGH4-ΔIC3B, isolated from *E. coli*, are identified as PA following m/z selection in the MS quadrupole of the NTSR1:lipid 11+ charge state (highlighted yellow) and collisional activation to dissociate PA and its homologues (m/z 700–760 Da). b, Lipidomics analysis of purified NTSR1 with three technical replicates reveals peaks at low m/z. MS/MS spectra of the precursor ion [M-H-1] at m/z 699.32 highlighted yellow, leads to definitive fragment ions at m/z 281 and 417 consistent with the structure of PA (36:2). c, Analogous lipidomics analysis of purified β_1AR from insect cells with three technical replicates. MS/MS spectra of the two [M-H-1] precursor ions (m/z 758.50 and 786.53) identified the lipids as PS (34:2) and PS (36:2) respectively with diagnostic fragments indicated.

Note on the strategy of the protocol to confirm lipid identities

Our methodology is not designed to identify all lipids that co-purify with receptors under different detergent environments. Rather we first identify those lipid classes that bind preferentially by directly detecting protein-lipid interactions by native MS and identifying the bound lipids through tandem MS. In our experiments two lipid classes were identified (PS and PIP) bound to all three receptors. Lipids with low affinity are ejected during collisional activation, during the removal of the detergent micelle in the MS, leaving only lipids with high binding affinity. Subsequently we incubate receptors with known concentrations of the lipids identified (from the PS and PIP classes) and use titration and competition experiments to identify PIP_2, from the PIP class, as the preferred interactor. We then investigate the effects of PIP_2 on the receptor structure and function.

Note on the composition of different membranes

The receptors used here were isolated either from insect cells or *E. coli* membranes raising concerns about the differences in composition between these cell membranes and those in mammalian systems. Several lipidomics studies of insect cell membranes have addressed the similar abundance of common phospholipids identified in mammalian membranes such as PE, PC, PI and cardiolipin[1] (ISSN 0014-5793). These lipids were also observed in our lipidomics analysis. Sphingolipids and sterols are also present in insect cell membranes although the types and structural features may differ from mammalian membranes. Cholesterol has been identified in several insect cell lines with a lower expression level than in mammalian cells (around 20-40% compared to mammalian cells)[2]. We did not observe any cholesterol bound to receptor or present in our lipidomics study. The impact of cholesterol on modulating GPCRs, especially their conformational stability, has been widely studied and cholesterol is often present in X-ray structures [3-5]. For example, the presence of cholesterol at the surface between TM1 to TM4 of β_2AR increases kinetic, energetic, and mechanical stability of receptor as well as potentially modulates receptor dimerization[3,4,6]. Furthermore, cholesterol increases the stability of NTSR1 in the detergent micelles but shows no effect when the receptor is reconstituted in lipid nanodiscs[7]. MD simulations indicate the highly dynamic nature of cholesterol binding hot-spots, suggesting that these sites have high occupancy rather than specific binding[8]. All these studies highlight the importance of the presence of cholesterol, however the detailed mechanism of its interaction remains inconclusive.

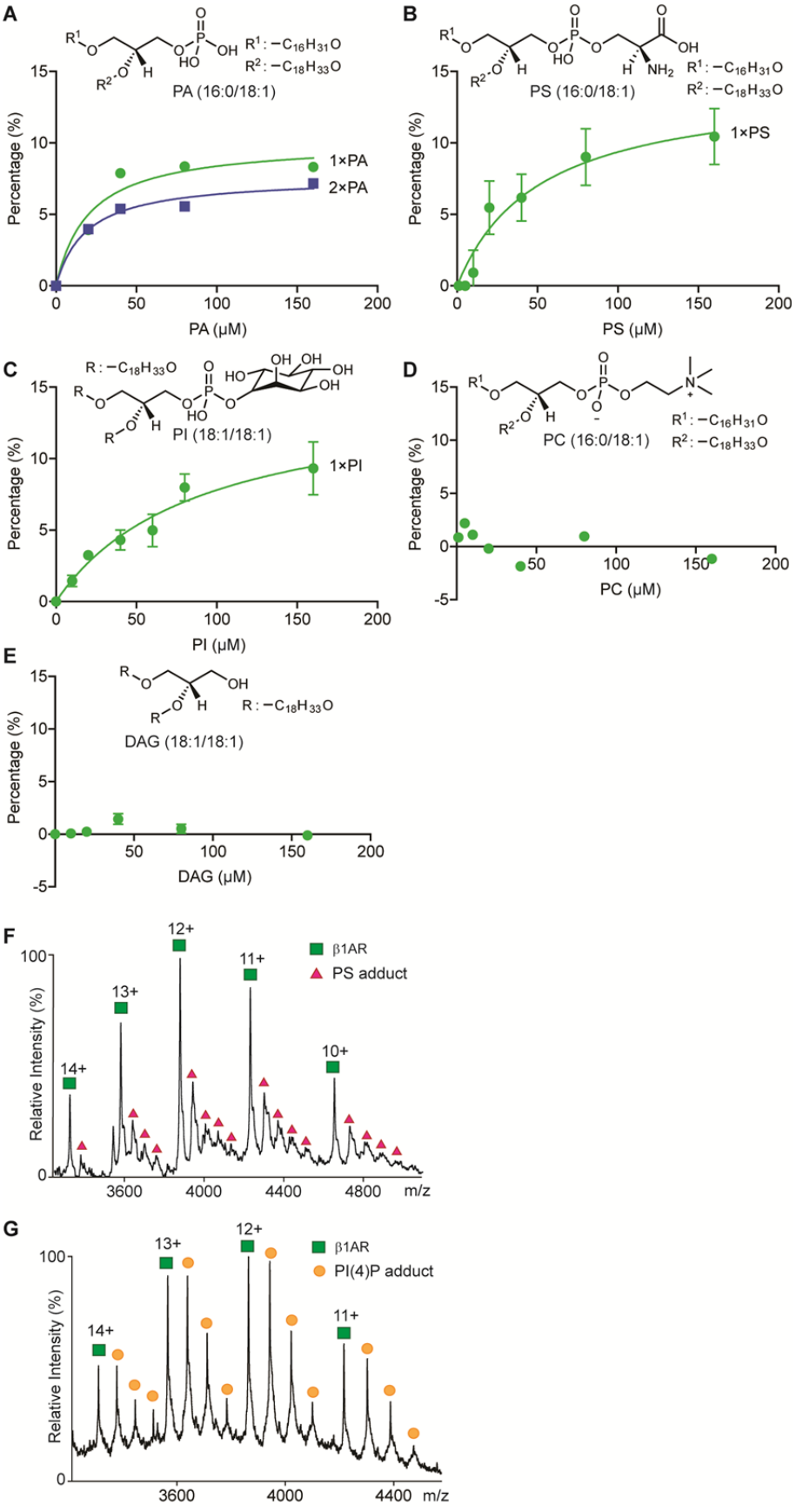
A
PA (16:0/18:1)
Percentage (%)
PA (μM)
1×PA
2×PA
B
PS (16:0/18:1)
PS (μM)
1×PS
C
PI (18:1/18:1)
PI (μM)
1×PI
D
PC (16:0/18:1)
PC (μM)
E
DAG (18:1/18:1)
DAG (μM)
F
β1AR
PS adduct
Relative Intensity (%)
m/z
G
β1AR
PI(4)P adduct

Extended Data Figure 2. Lipid binding preference of NTSR1 and β_1AR. The binding of NTSR1 HTGH4-ΔIC3B, measured by mass spectrometry (n=3), to the phospholipids PA (**a**), PS (**b**), PI (**c**), PC (**d**) and DAG (**e**). The measurements were performed at different lipid concentration (0 to160 μM) and the percentages of individual lipid-binding peaks (sum of apo protein and all lipid adducts obtained in the region of the mass spectrum under study) were plotted against lipid concentrations in solution. The lipid-binding curves were deduced from fitting to one-site total binding (GraphPad Prism software). Standard deviations of the mean were calculated from three independent replicate experiments at each concentration. The results show that NTSR1 interacts preferentially with anionic phospholipids (PA and PS) as no binding was observed for neutral (DAG) and zwitterionic (PC) lipids. Exogenous POPS (**f**) and PI(4)P (**g**) were added to β_1AR at different final concentrations (10 μM shown here). Spectra were recorded for a range of lipid concentrations from 0 – 80 μM for PS and 0 – 20 μM for PI(4)P. Peak intensities of the individual PI(4)P-bound species were measured and plotted against lipid concentration to yield a relative affinity for one PI(4)P binding (1x), two PI(4)P molecules binding (2x) or three PI(4)P molecules binding (3x); only the first PI(4)P molecule binds with high affinity (see Fig. 1a). Error bars represent the standard deviation of the mean between three independent experiments.

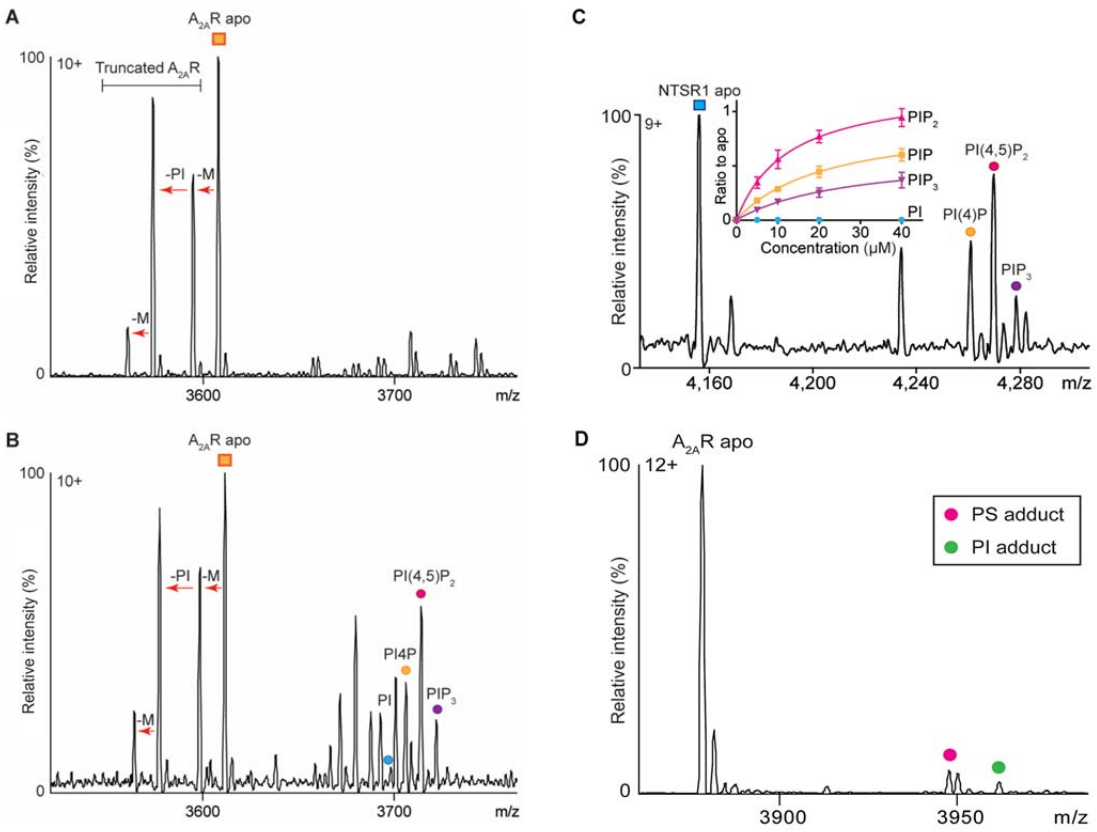

Extended Data Figure 3. Investigation of the phospholipid preferences of $A_{2A}R$ and NTSR1. a, A representative mass spectrum of purified $A_{2A}R$ from three independent experiments revealed truncations of the N-terminal sequence (MPIM). The arrow between each species refers to the mass differences corresponding to truncated amino acids (M, PI and M). **b,** A competitive binding assay (n=3) in which $A_{2A}R$ was incubated with a mixture of lipids (PI, PI(4)P, PI(4,5)P_2, and PI(3,4,5)P_3) prior to MS, indicated that PIP_2 binds with a higher affinity than other phospholipids to $A_{2A}R$. **c,** The analogous competitive binding assay in which NTSR1 was incubated with a mixture of lipids (PI, PI(4)P, PI(4,5)P_2, and PI(3,4,5)P_3) prior to MS. Ratio to apo is plotted as a function of concentration and defined as the intensity ratio of individual PIP adducts to the receptor in the apo state. The same data analysis methods are used for Fig. 1b. Results indicate that PIP_2 binds with a higher affinity than other phospholipids to $A_{2A}R$. Error bars represent standard deviation of the mean from three independent replicates. **d,** A representative mass spectrum of $A_{2A}R$ (n=3) used for preparation of the G protein complex reveals lower abundance of PS and PI adducts prior coupling to G proteins.

Note on the use CGMD Simulations of Protein-Lipid Interactions

The simulations use coarse-grained (CG) MD simulations with the Martini forcefield. This methodology is well established for the study of membrane proteins and their interactions with lipids[9,10]. The primary strength of the approach is long simulations are possible and so one can fully sample the interactions of membrane proteins with (slowly diffusing) lipids [11], which remains challenging for all atom simulations. Furthermore, the approach has been carefully validated for a number of membrane proteins whose lipid interactions are well understood experimentally (see below). Furthermore, recent studies from our group have suggested that atomistic force-fields may actually *overestimate* the strength of protein-lipid interactions and thus further work is need to refine these models[12]. The primary limitation of the CG method is one does not get full atomic resolution detail for the predicted interactions. However, when needed this can be obtained by a multiscale approach in which the CG structure is converted back to atomic resolution and an all atomic simulation then performed[13].

In terms of lipid specificity, we have previously employed two canonical membrane proteins, whose protein/lipid interactions have been characterised both structurally and functionally, namely: (i) the mitochondrial ATP/ADP transporter ANT1, which has three binding sites specific for cardiolipin seen in the crystal structure (CL); and (ii) inward rectifier potassium (Kir) channels the PIP_2 binding site of which has also been resolved at high resolution by X-ray crystallography. In both of these cases, we have demonstrated the ability of CGMD simulations to distinguish between specific and 'annular' lipid interactions, e.g. comparing the interactions of ANT with CL vs. PS or vs. PC [14] or of Kir channels with PIP_2 vs. PS[15].

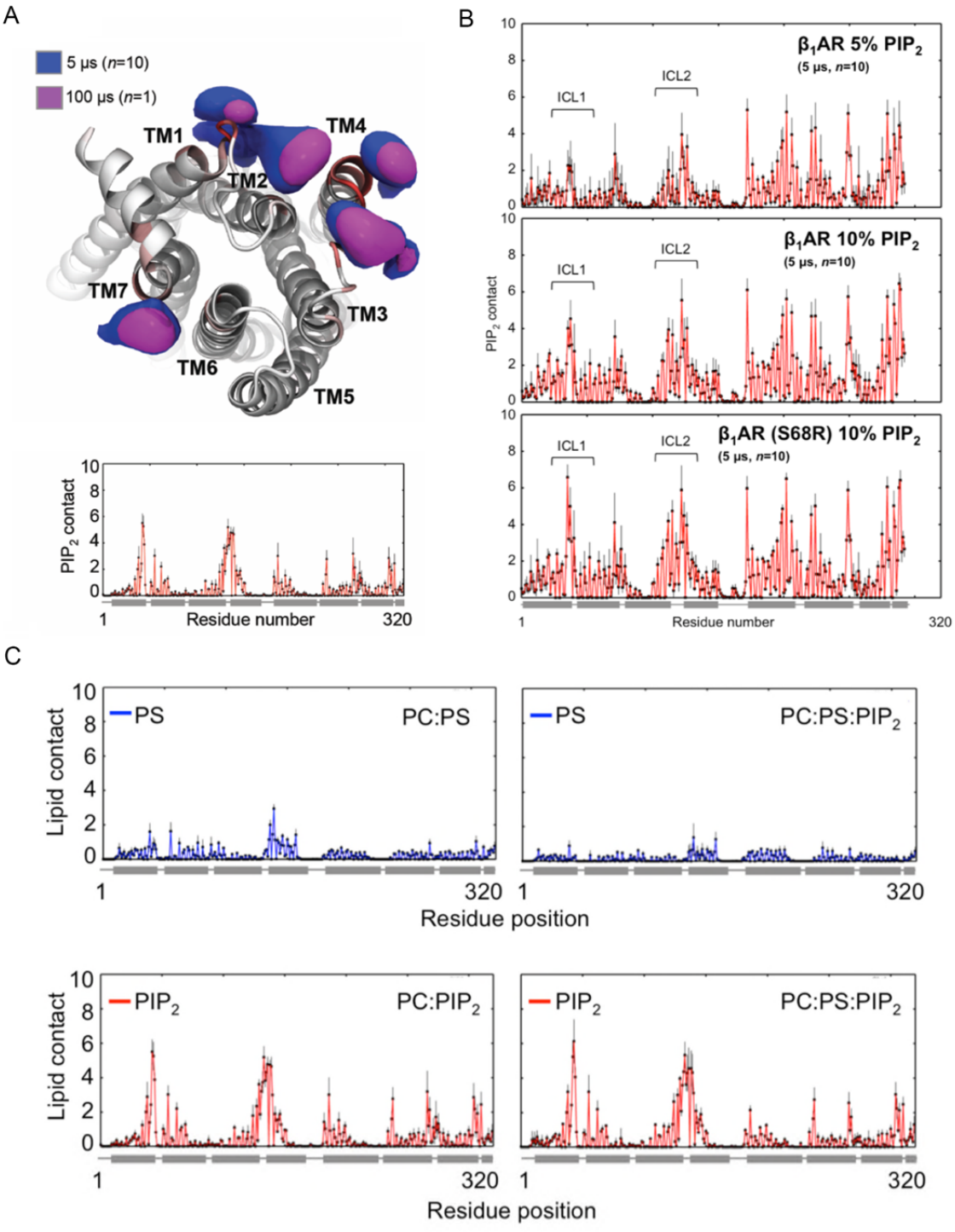
A
5 μs (n=10)
100 μs (n=1)
TM1
TM2
TM3
TM4
TM5
TM6
TM7
PIP2 contact
Residue number
1
320
B
β1AR 5% PIP2
(5 μs, n=10)
β1AR 10% PIP2
(5 μs, n=10)
β1AR (S68R) 10% PIP2
(5 μs, n=10)
ICL1
ICL2
PIP2 contact
Residue number
C
PS
PC:PS
PC:PS:PIP2
PIP2
PC:PIP2
PC:PS:PIP2
Lipid contact
Residue position

D

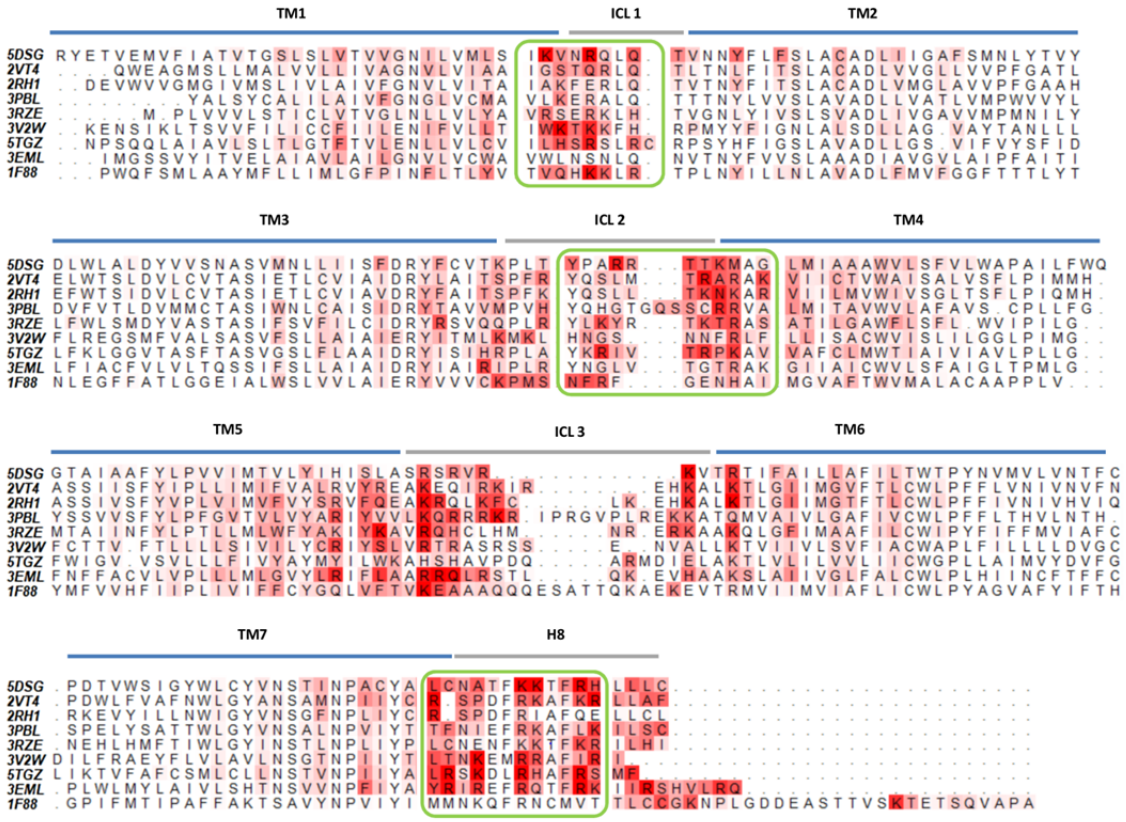

Extended Data Figure 4. NTSR1- and β_1AR-PIP$_2$ interactions within CGMD simulations and comparison of PIP$_2$ contacts over different GPCRs. a, Volumetric density surfaces showing the average spatial occupancy of PIP$_2$ lipids around a crystal structure of NTSR1 TM86V-ΔIC3B (PDB: 4BUO), which shares a greater sequence identity to the wild-type receptor (91%) than NTSR1 HTGH4-ΔIC3B (86%), contoured to show the major PIP$_2$ interaction sites. Density surfaces were calculated over 5-μs of CGMD (blue surface, n=10 independent experiments), and 100-μs of CGMD (magenta, n=1 independent experiment). The cytoplasmic side of NTSR1 structure is colored from white (low PIP$_2$ interaction) to red (high PIP$_2$ interaction). Extending a simulation to 100 μs revealed no overall change in the patterns of PIP$_2$ interaction. Less specific, and hence more dynamic, interaction was seen for the acyl chain moieties of PIP$_2$, which yielded more diffuse probability densities. **b,** β_1AR-PIP$_2$ interactions within CGMD simulations. Contact patterns are shown for simulations containing 5% PIP$_2$ in the lipid bilayer and thermostable β_1AR (PDB: 2Y03, upper panel), 10% PIP$_2$ and thermostable β_1AR (middle panel), and 10% PIP$_2$ and S68R β_1AR construct (bottom panel). In each case PIP$_2$ contacts were calculated over 5-μs of CGMD (n=10 independent experiments), with each repeat simulation initiated from different random system configurations. The std of the mean of lipid contact number is denoted by black error bars. **c,** PS and PIP$_2$ contacts with NTSR1 as a function of residue position, for PC:PS membranes (top left), PC:PS:PIP$_2$ membranes (top right), PC:PIP$_2$ membrane (bottom left) and PC:PS:PIP$_2$ (bottom right). The position of helices is denoted by horizontal grey bars. Lipid contact is calculated as

the mean number of contacts between each residue and a given lipid species per frame, using a 6 Å distance cut-off. Error bars (black) denote the standard deviation of the mean between simulation repeats (n=3). **d,** PIP_2 contacts seen in CG MD simulations for nine Class A GPCRs (3RZE = histamine H1 receptor; 2VT4 = β_1 adrenergic receptor; 2RH1 = β_2 adrenergic receptor; 5TGZ = CB1 cannabinoid receptor; 5DSG = M4 muscarinic acetylcholine receptor; 3EML = adenosine A_{2A} receptor; 3PBL = dopamine D3 receptor; 3V2W = sphingosine 1-phosphate receptor; 1F88 = rhodopsin). The sequences of the GPCRs are shown, with the TM helices, intracellular loops (ICL) and H8 helices indicated by horizontal bars, and with amino acids coloured by their mean number of contacts per simulation frame with the PIP_2 molecules. The three green boxes correspond to the high frequency of PIP_2 interactions discussed in the main text for the NTSR1, for the TM1, TM4, and TM7/H8 motifs. Contacts were computed over 1 μs CG-MD simulations (n=3 independent experiments) for each GPCR, using a 6 Å cut-off. Sequences were aligned using T-Coffee [16] and mapping of protein-lipid contact data onto the sequence alignment used ALINE[17].

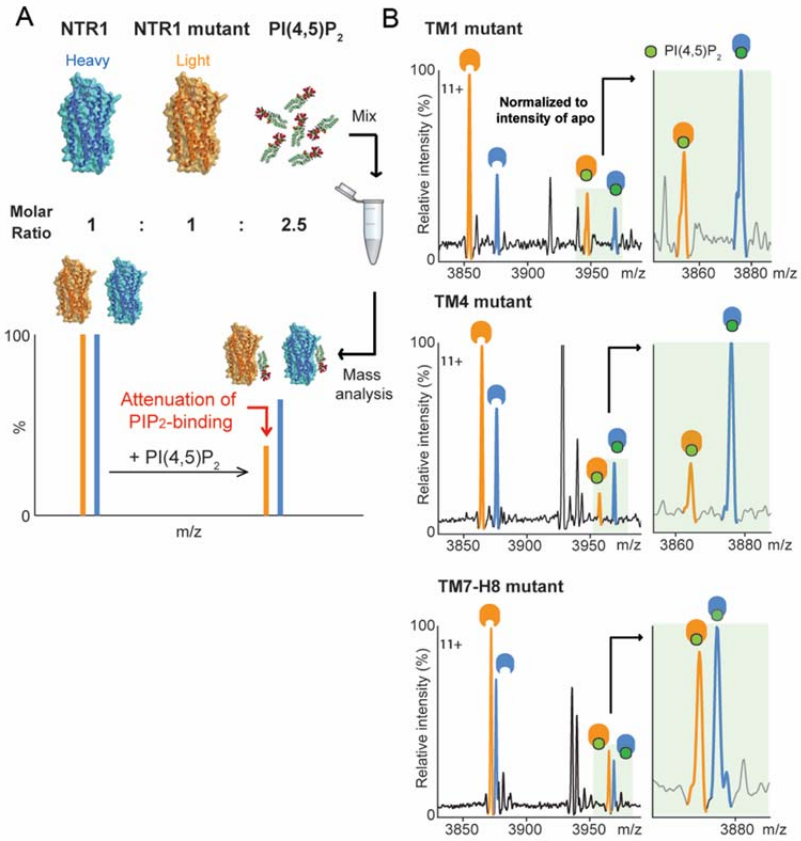

Extended Data Figure 5. Site-directed mutagenesis attenuates PIP_2 binding to NSTR1. a, Schematic representation of the experimental protocol designed to combine MS with mutagenesis to produce mutants of lower molecular mass than wild type which when incubated with PIP_2 yield a direct readout of the effect of mutations in specific regions. **b,** PIP_2-binding of NTSR1 mutants on residues that exhibit the highest frequency of PIP_2 interaction in MD simulation. Mutation of NTSR1 HTGH4-ΔIC3B residues on

TM1 (R46G, K47G and K48G (R43G, K44G and K45G in NTSR1 TM86-ΔIC3B; R91G, K92G, K93G in wild-type); red bar), TM4 (R138I, R140T, K142L and K143L (R135I, R137T, K139L and K140L in NTSR1 TM86-ΔIC3B; R183I, R185T, K187L and K188L in wild-type); orange bar) and TM7-H8 (R316N (R311N in NTSR1 TM86-ΔIC3B; R377N in wild-type); green bar) attenuate PIP_2 binding, and indicates that the TM4 interface is a preferential binding site over TM1 and TM7-H8 interfaces. The selection of residues for mutations was guided by MD (Extended Data Figure 4) and previous studies wherein binding of a fluorescence-labeled agonist, BODIPY neurotensin, to NTSR1, was screened and used to monitor efficient production, insertion, and folding.[18]

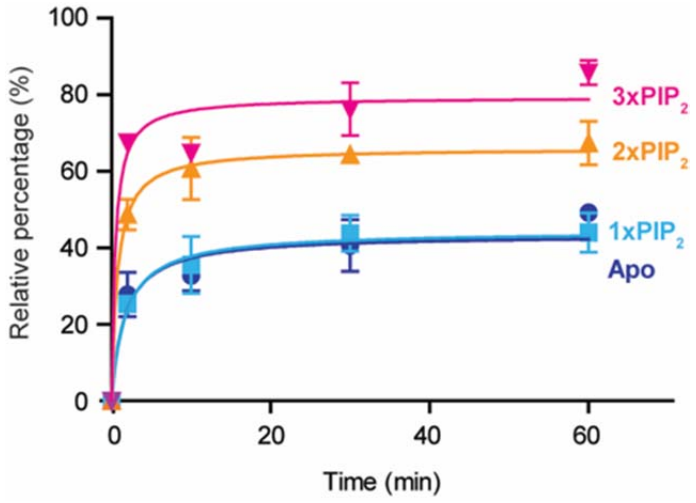

Extended Data Figure 6. PIP_2 stabilises β_1AR coupled to mini-G_s. A time course experiment was performed to capture the complex formation of mini-G_s and active β_1AR as a function of time. The coupling efficiency (percentage) was calculated from the relative intensity of peaks assigned to the β_1AR coupling to mini-G_s at the appropriate lipid-bound state. The plot indicates that mini-G_s coupling is enhanced by PIP_2 when more than two lipids are bound to the receptor. Error bars represent standard deviations of the mean from at least three independent experiments.

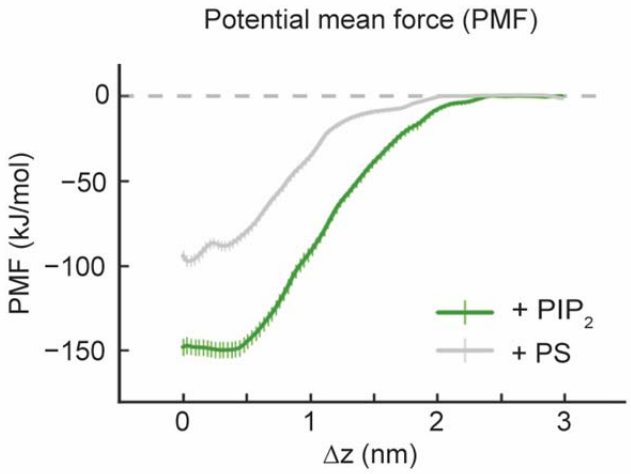

Extended Data Figure 7. PIP_2 stabilises the $A_{2A}R$-mini-G_s complex. Plot of potential of mean force (PMF) for the interaction of mini-G_s with $A_{2A}R$ in the presence of PIP_2 (green curve) and PS (grey). The PMF is calculated along a reaction coordinate (Δz) corresponding to the centre-centre separation of the mini-G_s and receptor proteins along the z-axis (normal to the bilayer plane). The interaction of mini-G_s with the $A_{2A}R$ is stabilised in the presence of PIP_2 by ~50 ± 10 kJ/mol relative to PS. The error bars on the figure (which are less than 10 kJ/mol) are from bootstrap sampling of the PMFs and thus are the 'statistical' errors in estimating the well depth from a given set of simulations/PMF calculation (n=3 independent experiments). A minimum error of <= ~10 kJ/mol is therefore estimated.

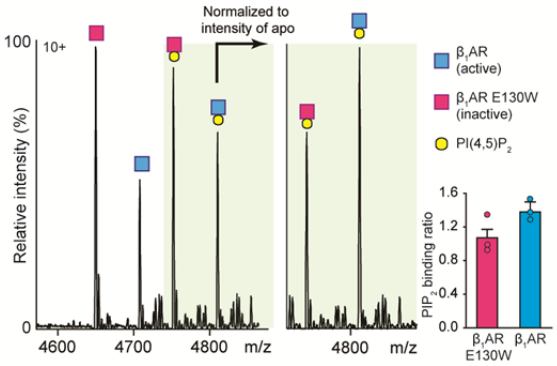

Extended Data Figure 8. PIP_2 binds preferentially to β_1AR in an active state. Mass spectra were recorded for a 1:1 equimolar mix of an inactive unliganded β_1AR variant E130W and its unmodified active counterpart (co-purified with the agonist isoprenaline) in the presence of $PI(4,5)P_2$. Lipid binding occurred on both receptors but following normalization to account for differences in ionization efficiency a clear preference for PIP_2 binding to the active receptor was observed. (Error bars denote standard deviation of the mean between three independent experiments).

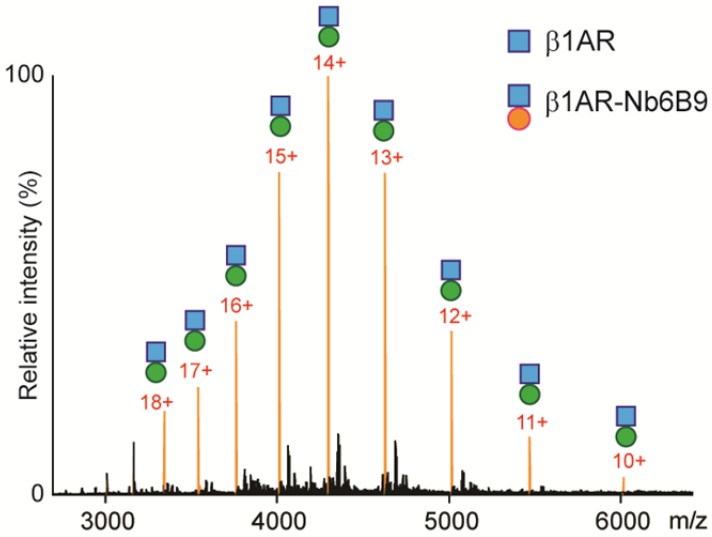

Extended Data Figure 9. Detection of nanobody coupling to β_1AR. Mass spectral peaks assigned to the nanobody (Nb6B9) binding to β_1AR to form a β_1AR·Nb6B9 complex at an equimolar ratio are highlighted (orange) and demonstrate complete complex formation implying a higher affinity of the nanobody than mini-G_s for β_1AR (N=3 independent experiments)**.**

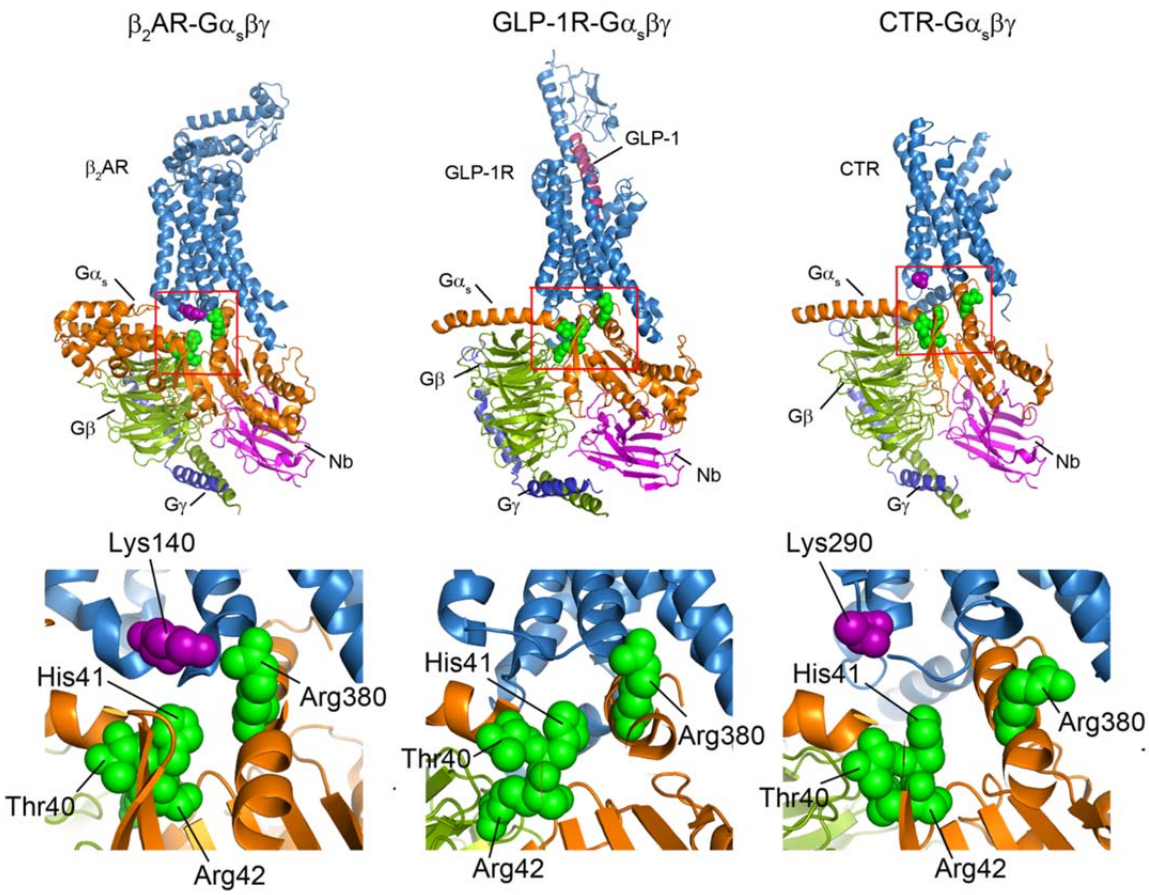

Extended Data Figure 10. Structural comparison of class A and class B GPCRs in complex with trimeric Gαβγ complexes. The PIP_2 contacts of the $G\alpha_s$ subunit observed in MD simulation (green spheres) were highlighted on the structures of trimeric G interactions with β_2-adrenergic receptor (β_2AR) (PDB: 3SN6), the glucagon-like peptide-1 receptor (GLP-1) (PDB: 5VAI), and the calcitonin receptor (CTR) (PDB: 5UZ7). The basic residues on the interface adjacent to the cytoplasmic end of TM4 are also highlighted (purple spheres). Expansion indicates the conserved pattern of PIP_2 bridging in class A GPCRs (β_2AR and A_{2A}R (Fig. 3e)) both of which have basic residues on TM4 (Lys140 and Arg107/111) which are not observed in class B GPCRs GLP-1R and CTR.

Table 1. Lipidomics anaylsis of purified β_1AR

Mass (Da)	Lipid ID
824.61	PC (36:0)
716.52	PE (34:1)
742.54	PE (36:2)
714.51	PE (34:2)
772.59	PE (38:1)
752.57	PE (37:4)
793.57	PG (38:6)
807.50	PI (32:1)
833.52	PI (34:2)
865.58	PI (36:0)
835.53	PI (34:1)
863.57	PI (36:1)
861.55	PI (36:2)
891.60	PI (38:1)
758.50	PS (34:2)
760.51	PS (34:1)
786.53	PS (36:2)
1019.60	PIP (42:5)
1343.90	CL (64:4)
1371.93	CL (66:4)
1399.96	CL (68:4)

Table 2. Simulations run. Lipids were symmetrically distributed between leaflets.

Name	Length	Bilayer Composition
NTSR1	10 x 5 μs	POPC(95%):PIP_2(5%)
NTSR1	3 x 5 μs	POPC(95%):PS(5%)
NTSR1	10 x 5 μs	POPC(95%):PS(5%):PIP_2(5%)
NTSR1 extended	1 x 100 μs	POPC(95%):PIP_2(5%)
β_1AR (5%)	10 x 5 μs	POPC(95%):PIP_2(5%)
β_1AR (10%)	10 x 5 μs	POPC(90%):PIP_2(10%)
β_1AR (S68R, 10%)	10 x 5 μs	POPC(90%):PIP_2(10%)
A_{2A}R-mini-G_S	10 x 8 μs	POPC(95%):PIP_2(5%)

References

1 Marheineke, K., Grunewald, S., Christie, W. & Reilander, H. Lipid composition of Spodoptera frugiperda (Sf9) and Trichoplusia ni (Tn) insect cells used for baculovirus infection. *FEBS Lett* **441**, 49-52, (1998).

2 Hafer, A., Whittlesey, R., Brown, D. T. & Hernandez, R. Differential incorporation of cholesterol by Sindbis virus grown in mammalian or insect cells. *J. Virol* **83**, 9113-9121, (2009).

3 Cherezov, V. *et al.* High-resolution crystal structure of an engineered human beta2-adrenergic G protein-coupled receptor. *Science* **318**, 1258-1265, (2007).

4 Hedger, G. & Sansom, M. S. P. Lipid interaction sites on channels, transporters and receptors: Recent insights from molecular dynamics simulations. *Biochimica et Biophysica Acta- Biomembranes* **1858**, 2390-2400, (2016).

5 Guixa-Gonzalez, R. *et al.* Membrane cholesterol access into a G-protein-coupled receptor. *Nat. Commun.* **8**, 14505, (2017).

6 Zocher, M., Zhang, C., Rasmussen, S. G., Kobilka, B. K. & Muller, D. J. Cholesterol increases kinetic, energetic, and mechanical stability of the human beta2-adrenergic receptor. *Proc. Natl. Acad. Sci. U. S. A.* **109**, E3463-3472, (2012).

7 Oates, J. *et al.* The role of cholesterol on the activity and stability of neurotensin receptor 1. *Biochim Biophys Acta* **1818**, 2228-2233, (2012).

8 Sengupta, D. & Chattopadhyay, A. Molecular dynamics simulations of GPCR-cholesterol interaction: An emerging paradigm. *Biochim Biophys Acta* **1848**, 1775-1782, (2015).

9 Marrink, S. J. & Tieleman, D. P. Perspective on the Martini model. *Chem. Soc. Rev.* **42**, 6801-6822, (2013).

10 Hedger, G. & Sansom, M. S. P. Lipid interaction sites on channels, transporters and receptors: recent insights from molecular dynamics simulations. *Biochim. Biophys. Acta* **1858**, 2390–2400, (2016).

11 Domański, J., Hedger, G., Best, R., Stansfeld, P. J. & Sansom, M. S. P. Convergence and sampling in determining free energy landscapes for membrane protein association. *J. Phys. Chem. B.* **121**, 3364–3375, (2017).

12 Domański, J., Sansom, M. S. P., Stansfeld, P. J. & Best, R. B. Balancing protein-lipid interactions to capture transmembrane helix-helix association. . *J. Chem. Theor. Comput.* **(minor revisions submitted)**, (2018).

13 Stansfeld, P. J. & Sansom, M. S. P. From coarse-grained to atomistic: a serial multi-scale approach to membrane protein simulations. *J. Chem. Theor. Comp.* **7**, 1157–1166, (2011).

14 Hedger, G. *et al.* Lipid loving ANTs: molecular simulations of cardiolipin interactions and the organization of the adenine nucleotide translocase in model mitochondrial membranes. *Biochemistry* **55**, 6238–6249, (2016).

15 Schmidt, M. R., Stansfeld, P. J., Tucker, S. J. & Sansom, M. S. P. Simulation-based prediction of phosphatidylinositol 4,5-bisphosphate binding to an ion channel. *Biochem.* **52**, 279-281, (2013).

16 Notredame, C., Higgins, D. G. & Heringa, J. T-coffee: a novel method for fast and accurate multiple sequence alignment11Edited by J. Thornton. *J. mol. biol.*

302, 205-217, (2000).
17 Bond, C. S. & Schuttelkopf, A. W. ALINE: a WYSIWYG protein-sequence alignment editor for publication-quality alignments. *Acta Crystallographica Section D* **65**, 510-512, (2009).
18 Schlinkmann, K. M. *et al.* Critical features for biosynthesis, stability, and functionality of a G protein-coupled receptor uncovered by all-versus-all mutations. *Proc. Natl. Acad. Sci. U. S. A.* **109**, 9810-9815, (2012).